

AD-A100 827 AIR FORCE INST OF TECH WRIGHT-PATTERSON AFB OH SCH00--ETC F/G 10/2
PRIME POWER TO PULSE CONDITIONING INTERFACE METHODS.(U)
DEC 80 J R SILVA
UNCLASSIFIED AFIT/6E/EE/80D-39

NL

1 OF 1
AD A
100827

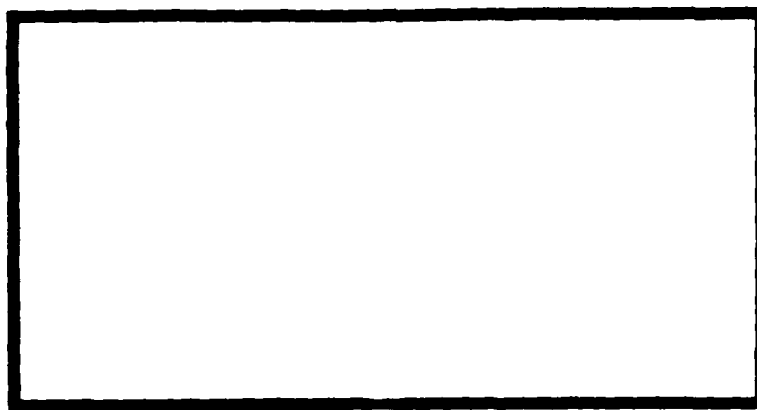
END
DATE
FILMED
7-81
DTIC

Doc

AD A100827



LEVEL II



DTIC FILE COPY

UNITED STATES AIR FORCE
AIR UNIVERSITY
AIR FORCE INSTITUTE OF TECHNOLOGY
Wright-Patterson Air Force Base, Ohio

DTIC
ELECTE
JUL 1 1981
S D

DISTRIBUTION STATEMENT A

Approved for public release;
Distribution Unlimited

81 6 30 032

AFIT/GE/EE/80D-39

Accession For	
NTIS GRA&I	X
DTIC TAB	
Unannounced	
Justification	
By	
Distribution	
Availability	
Dist	
A	

PRIME POWER TO PULSE CONDITIONING
INTERFACE METHODS
THESIS
AFIT/GE/EE/80D-39, Jaime R. Silva
2d LT USAF

Approved for public release; distribution unlimited.

AFIT/GE/EE/80D-39

PRIME POWER TO PULSE CONDITIONING
INTERFACE METHODS

THESIS

Presented to the Faculty of the School of Engineering
of the Air Force Institute of Technology
Air Training Command
in Partial Fulfillment of the
Requirements for the Degree of
Master of Science

by

Jaime R. Silva, B.S.

2d LT USAF

Graduate Electrical Engineering

December 1980

Preface

This thesis project was conducted not only as a part of the requirements for a masters program degree, but hopefully to make an immediate contribution to a current Air Force and Army joint program for the design of power supplies for future directed energy weapons.

I am most grateful to my professor and thesis advisor Captain Fred Brockhurst for his guidance during all phases of this thesis work. His willingness and ability to help me made possible this report.

The hardware tests were conducted at the Electrical Equipment Division U.S. Army Mobility Equipment Research and Development Command (MERADCOM), Fort Belvoir, Virginia. Since this was my first working experience, not much would have been done without the help and cooperation of the following people from MERADCOM.

I would like to express my gratitude to my advisors Dr. Alois L. Jokl and Dr. Larry I. Amstutz who gave me confidence and constant encouragement to carry on with this task. The test system was assembled by Mr. David Presley who assisted me during the experimental portion of the project. His knowledge and experience proved useful, especially when Murphy's law manifested itself, saving me much time and effort. Special acknowledgement is due to Mr. James Ferrick who provided constructive criticism and stimulating discussion on almost every aspect of this project.

Jaime R. Silva

Table of Contents

	<u>Page</u>
Preface	ii
List of Figures	
List of Tables.	
Abstract	
I. Introduction	1
Background.	1
Problem	1
Scope	2
II. DC Resonant Charging	3
Theory - Introduction	3
Analysis of Voltage Sagging	4
Computer Programs	6
Effect of Voltage Sagging	8
Experimental Equipment & Instrumentation.	20
Description of Pulser	24
Modifications Made to the Pulser.	26
Operation of Pulser	27
General Approach.	27
Results - Prime Power System.	29
Generator	29
Vibration & Heating	29
Voltage Regulator	29
Sag on Output Voltage	32
Pulser Performance.	36
Network Voltage & Charging Current.	36
Resonance Frequency	38
III. AC Resonant Charging	40
Theory - Introduction	40
Analysis	40
Experimental Equipment & Instrumentation.	42
Description of Pulser	44
Operation of Pulser	44
Results - Resonance Frequency	47
IV. Conclusions & Recommendations.	50
Recommended Additional Work	51
DC Resonant Charging.	51
AC Resonant Charging.	51

Table of Contents

	<u>Page</u>
Bibliography	52
Appendix A: Mathematical Analysis of DC Resonant Charging.	A-53
Appendix B: Computer Programs	B-56
Appendix C: Additional Case	C-62
Appendix D: Major Parts List.	D-64
Vita	65

List of Figures

<u>Figure</u>		<u>Page</u>
1	Equivalent DC Resonant Circuit	4
2	Plot of Average Input Power vs. Sag Constant .	7
3	Plot of Capacitor Voltage vs Time for 0% Sag .	8
4	Theoretical Plot of Maximum Capacitor Voltage vs Sag Constant.	9
5	Theoretical Plot of Resonance Frequency vs Sag Constant	10
6	Theoretical Plot of Average Power vs Sag Constant	11
7	Theoretical Plot of Peak Charging Current vs Sag Constant	12
8	Theoretical plots of the Charging Current and Capacitor Voltage for 0% Sag on Input Voltage.	15
9	Theoretical Plots of the Charging Current and Capacitor Voltage for 10% Sag on Input Voltage	16
10	Theoretical Plots of Charging Current and Capacitor Voltage for 15% Sag on Input Voltage	17
11	Theoretical Plots of the Charging Current and the Capacitor Voltage for 30% Sag on Input Voltage.	18
12	Theoretical Plots of the Charging Current and the Capacitor Voltage for 45% Sag on input Voltage.	19
13	Block diagram of DC Resonant Charging System .	20
14	DC Resonant Circuit.	21
15	Test Circuit Showing the Test Points	22
16	Schematic of Generator Instrumentation	25
17	Schematic Diagram of the DC Pulser	25
18	Scope Traces	30
19	Scope Traces	31

<u>Figure</u>		<u>Page</u>
20	Scope Traces	52
21	Scope Traces	53
22	Scope Traces	53
23	Scope Traces	54
24	Scope Traces	55
25	Scope Traces	57
26	AC Charging Circuit.	57
27	Block Diagram of AC Resonant Charging System	42
28	AC Resonant Circuit.	43
29	Schematic Diagram of AC Pulser	45
30	Scope Traces	48
A-1	Plot of Eq(1) for Two Charging Cycles . .	A-55
B-1	Fortran Program for Varying Sag Constant .	B-58
B-2a	Fortran Program for Charging Current and Capacitor Voltage Waveforms (Sheet 1 of 2)	B-59
B-2b	Fortran Program for Charging Current and Capacitor Voltage Waveforms (Sheet 2 of 2)	B-60
C-1	Scope Trace of DC Bus Voltage (TOP) and Charging Current (5 KV/div, 2A/div). . . .	C-62
C-2	Scope Trace of DC Bus Voltage (TOP) and Capacitor Voltage (5 KV/div)	C-65

List of Tables

<u>Table</u>		<u>Page</u>
1	Example of Pulser Performance for 0% and 48% Sag	13
2	Comparison of Calculated Values vs Actual Values.	39

Abstract

AC and DC resonant charging hardware tests were conducted with a 15KW DOD standard 400 HZ generator as prime power. DC resonant charging caused vibrations of the generator at the pulsing frequency and instability of the voltage regulator due to the very irregular generator voltage waveform. The input DC voltage to the pulser sagged causing the performance to be lower than expected. An analysis of this problem and the theory to account for this sag is presented.

Problems with the triggering of AC resonant charging were not solved in time for this report. The experimental set up of AC resonant charging is presented. AC resonant charging caused no negative impact on the generator which is a great advantage over DC resonant charging.

1. Introduction

Background

This project is a study of the interface between prime power systems and pulse conditioning systems for the use in electrical power generation for future directed energy systems.

The Army and the Air Force are sponsoring university work for the development of computerized theoretical predictions. The results of this thesis investigation will be used to refine and validate computer predictions which may then be used by Army and Air Force scientists as design aids for the power supplies required in directed energy systems.

The pulser used for these tests was constructed by Army's ERADCOM and contained separate sections for AC and DC resonant charging.

Each section contained the resonant circuit, support equipment, and controls.

Problem

There are several approaches to the interface between prime power generating equipment and pulse conditioning equipment. This is a study of two design approaches, these are DC resonant charging and AC resonant charging.

General areas to be observed are the impact on the prime power equipment of the charging scheme used and the performance of the charging method with this particular

kind of prime power source. Attention is given to grounding methods, electro-magnetic phenomena, physical layout of the components, and control requirements.

Scope

A laboratory set up was assembled using a 150W 50/60 standard 400HZ generator to try out each of the charging methods. These set ups included appropriate controls. Each system was instrumented so actual performance could be compared with present theory.

A mathematical analysis was done for the DC resonant charging method and the resulting equations were used in two computer programs. These computer programs provided the theoretical solutions to which observed performance was compared.

The AC resonant charging theory is discussed and the experimental set up described. No data was collected for AC resonant charging since problems with the triggering logic were not solved in time for this report. Several observations on AC resonant charging are included.

II. DC Resonant Charging

Theory

Introduction

The theory of DC resonant charging circuits has long been developed and circuits of this kind used for many years. The problem studied here was the effect of DC resonant charging on the prime power equipment of a possible power supply for directed energy weapons. The prime power source was a three phase system composed of a generator, a transformer, and a full wave bridge rectifier.

When a generator has a rectified load its voltage waveform is deformed by the commutation of the current on the rectifiers. In this case the load is also varying as a series of half sines and to make matters worse the discharge pulsing is reflected back on the generator waveform. This irregular current waveform causes additional heat losses in the generator windings and throughout the prime power system. The generator also vibrates at the pulsing frequency, this is so because the torque is proportional to the load current.

The output voltage from the prime power system was observed to drop proportional to the load current, or sag, during each charging cycle. A mathematical approximation of this characteristic was done and a complete analysis of its effect on the pulser performance was made.

This analysis is presented next, then theoretical results obtained from two computer programs are presented. These computer programs were developed using the equations obtained from the mathematical analysis.

Analysis of Voltage Sagging

The sagging on the output voltage during one charging cycle is determined by the generator and transformer reactance and the load current. The voltage regulator does not respond fast enough in that time period to make any changes in the shape of this sag. It is not discussed here how to determine the magnitude of this voltage sagging for a given system. However, the effect of this sagging on the pulser performance is studied in depth.

A DC resonant charging circuit can be represented as in Figure 1 below.

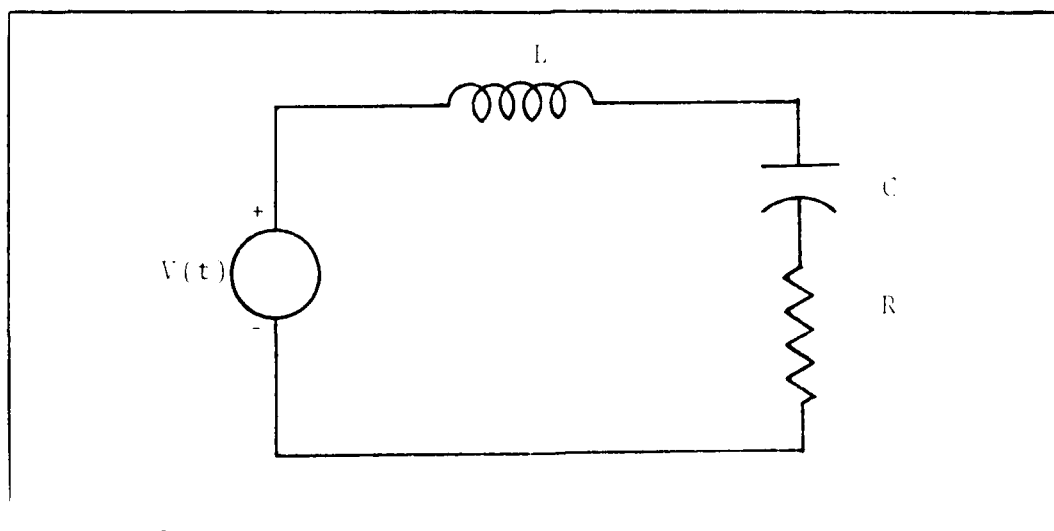


Figure 1 Equivalent DC Resonant Circuit

In Figure 1 L is the charging inductance, C is the total network capacitance and R is the sum of the charging inductor resistance and the equivalent load resistance.

The input voltage $V(t)$ was represented for this analysis as in Equation 1.

$$V(t) = E_{bb} (1 - K i_c(t)) \quad (1)$$

where E_{bb} is the peak input voltage, K is a constant, and $i_c(t)$ is the charging current as a function of time.

A mathematical analysis for the circuit of Figure 1 with an input voltage as given by Equation 1 is included in Appendix A. This analysis resulted in the following equations for the charging current and the capacitor voltage respectively.

$$i_c(t) = \frac{E_{bb} - V_o}{WL} e^{-bt} \sin w t + I_o e^{-bt} \left(\cos w t - \frac{b}{w} \sin w t \right) \quad (A-5)$$

$$V_c(t) = E_{bb} - (E_{bb} - V_o) e^{-bt} \left(\cos w t + \frac{b}{w} \sin w t \right) + \frac{I_o}{wC} e^{-bt} \sin w t \quad (A-6)$$

where,

V_o initial capacitor voltage

I_o initial inductor current

$b = \frac{R+K E_{bb}}{2L}$

$w = \left(\frac{1}{LC} - b^2 \right)^{\frac{1}{2}} = \text{circuit resonance frequency}$

The pulser resonance repetition frequency is two times the circuit resonance frequency given above. From now on, every time resonance frequency is mentioned it is referring to the pulser frequency.

Equations (A-5) and (A-6), and other equations derived in Appendix A were used to develop two interactive fortran programs to calculate the theoretical results.

Computer Programs

Two computer programs were developed as an aid in producing theoretical results. These were also used to test the effects of changes in the system parameters. Appendix B contains a copy of each program and a brief description of how they work.

The first program calculated the peak voltage in the capacitor, peak charging current, resonance frequency, and average power for increasing values of input voltage sag. This was calculated for a given circuit and voltage level. This data was used as input to a plotting routine and plots of the mentioned parameters versus the sag on the input voltage were obtained. An example of these plots is shown in Figure 2.

For example, the sag constant on the horizontal axis of Figure 2 is 0.2 for 20% sagging on the input voltage, 0.45 for 45%, and so on.

These plots were useful to indicate the difference in performance for different magnitudes of voltage sagging.

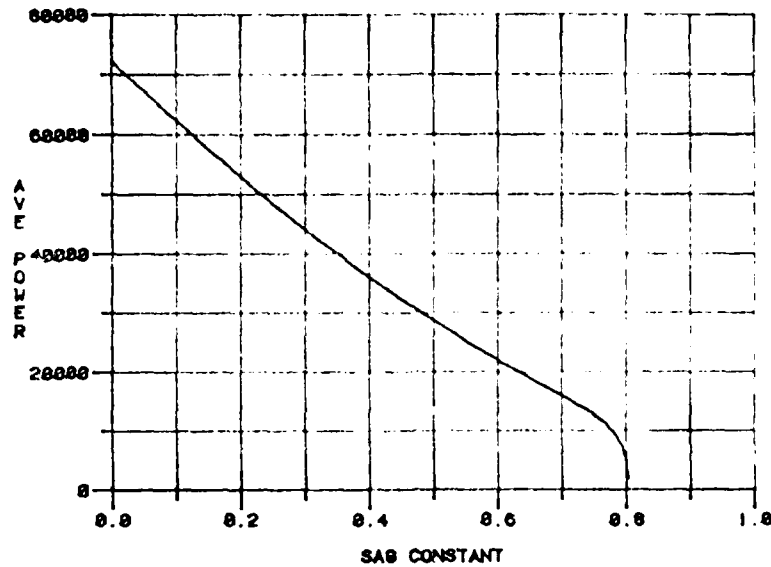


Figure 2 Plot of Average Input Power vs. Sag Constant

The second computer program used Equations (A-5) and (A-6) to generate a set of values for charging current and capacitor voltage versus time. The same plotting routine was then used to obtain the theoretical plots; these plots were used to compare to actual waveforms. Figure 3 on next page shows a plot obtained with this second program. The waveform shown in for the ideal case where the input voltage is a constant DC voltage.

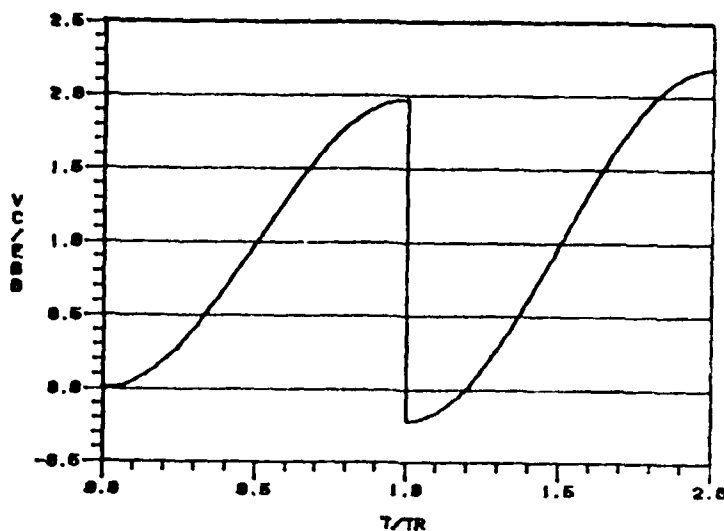


Figure 3 Plot of Capacitor Voltage vs. Time for 0% Sag

Effect of Voltage Sagging

For a constant input voltage the pulser would perform as predicted by Glasoe and Lebacqz (Ref 1, Chap 9). This case is shown in Figure 3 above. When the input voltage sags it is intuitive to say that the capacitor will charge to a lower voltage and that it will take a longer time to do so compared to the ideal case. In fact that is what happens in reality and the mathematical analysis reflects just that.

Figure 4 through 7 show how the maximum voltage in the capacitor, the resonance frequency, average power, and peak charging current will decrease as the magnitude of the sag increases. These plots are for a circuit with $L=2.9 \mu\text{H}$, $C=2.58 \mu\text{F}$, $R=17.5 \Omega$, $V_{ob}=10\text{KV}$, and $V_o = -0.1 V_c(T_p)$. Results from Figures 4 through 7 for the ideal case and 48% sag are summarized in Table 1 on page 13.

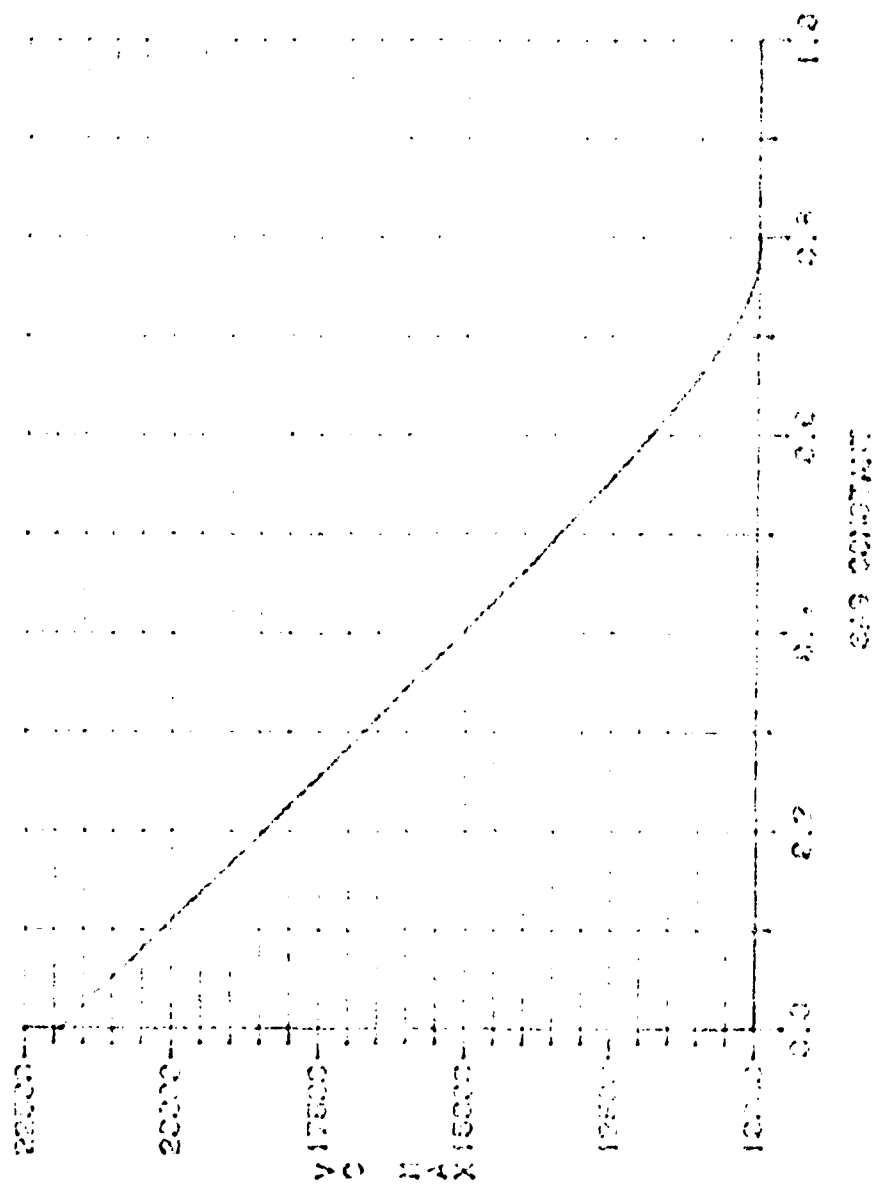


Figure 4 Theoretical Plot of Maximum Capacitor Voltage vs. Sag Constant

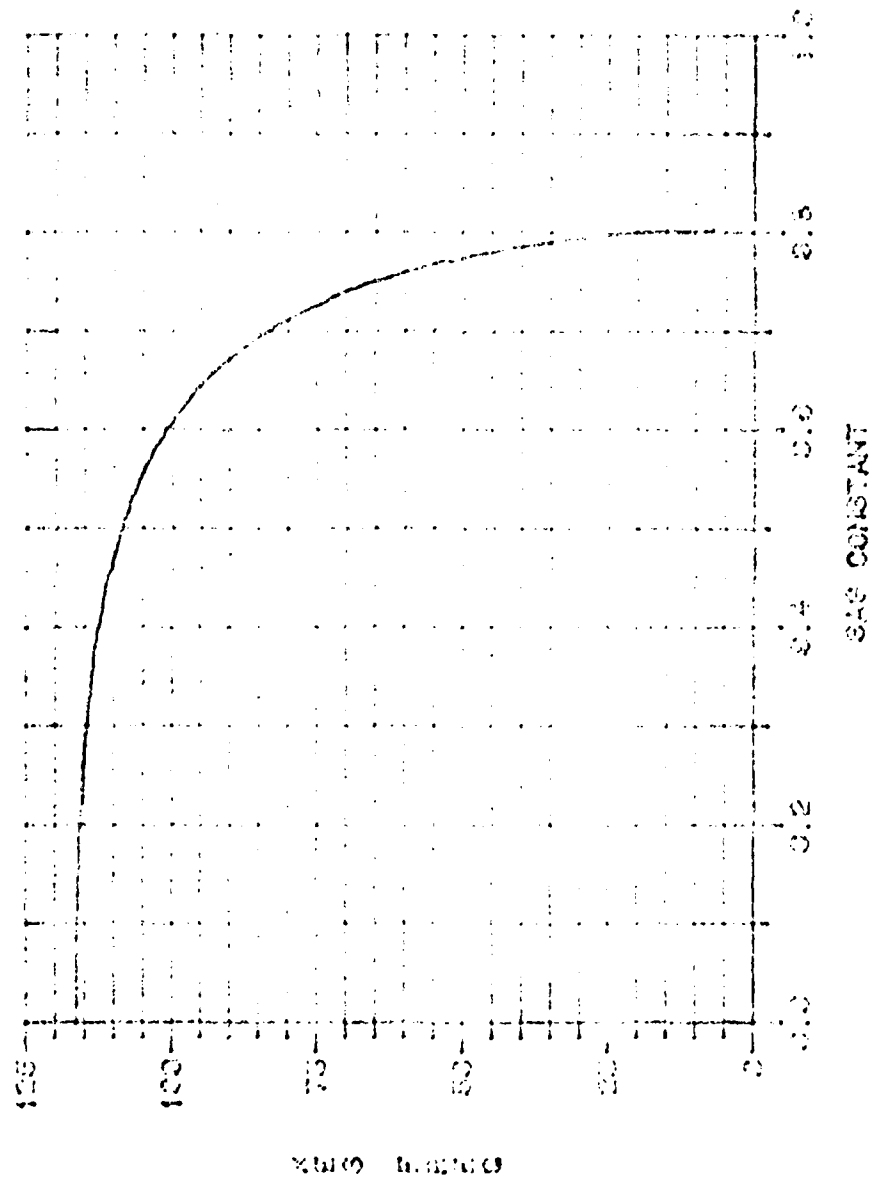


Figure 5 Theoretical Plot of Resonance Frequency vs. Sag Constant

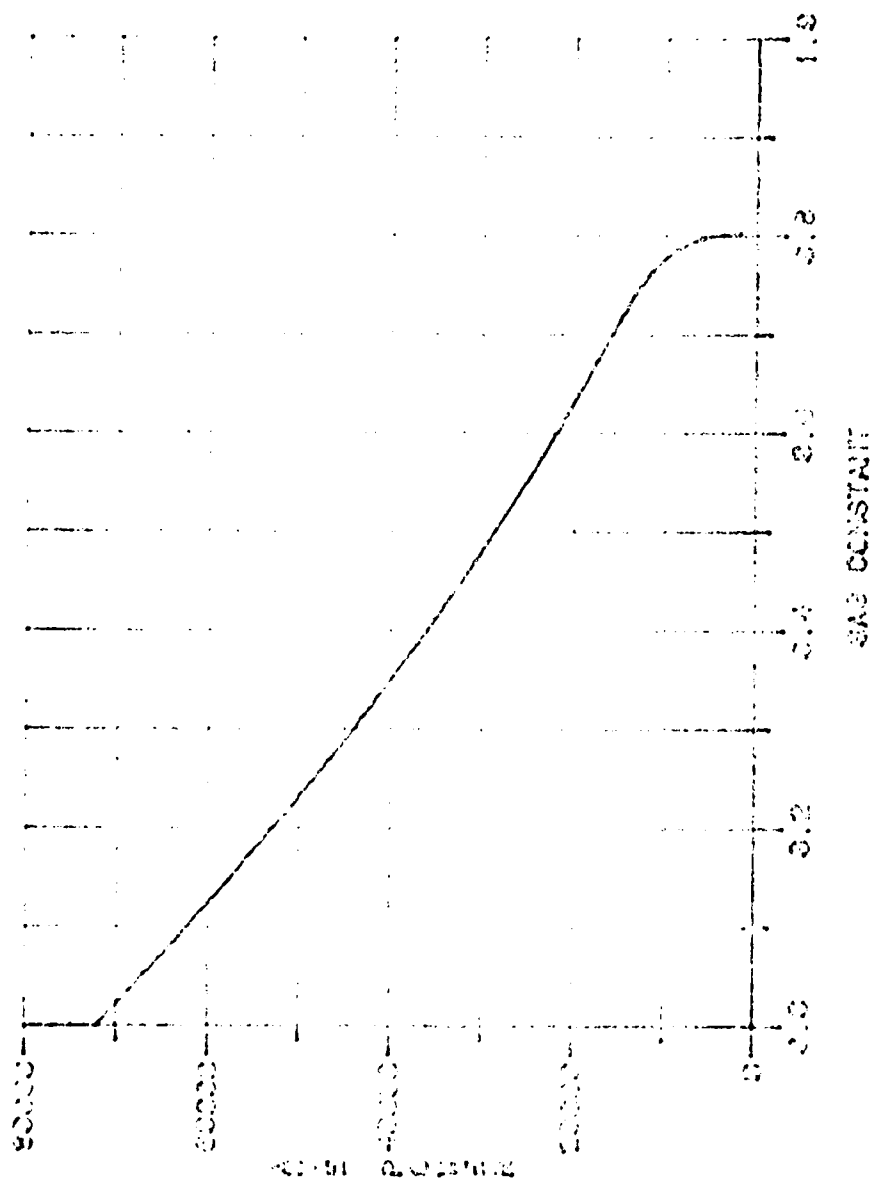


Figure 6 Theoretical Plot of Average Power vs.
Sag Constant

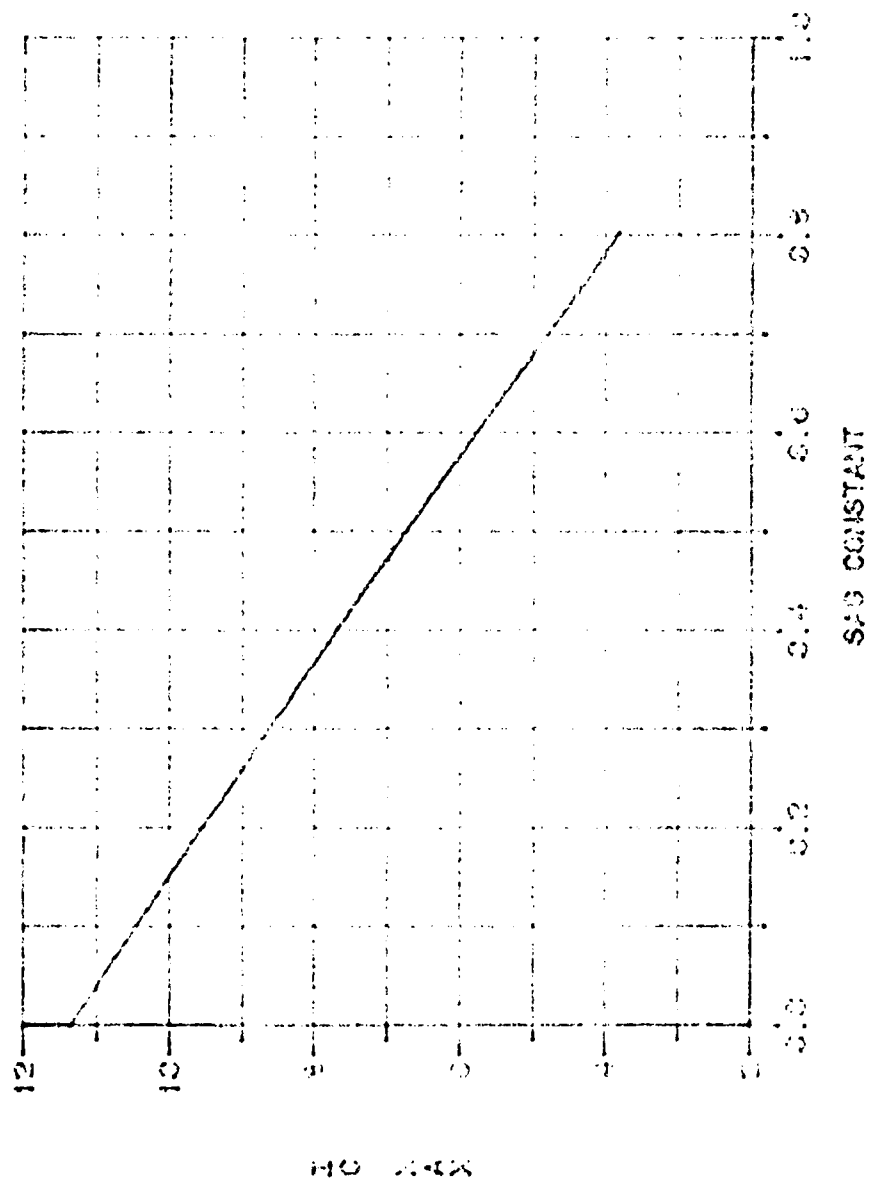


Figure 7 Theoretical Plot of Peak Charging Current vs. Sag Constant

Table 1 Example of Pulser Performance for
Sag Constant of 0.0 and 0.48

% SAG	W	$V_c(T_r)$	P_{av}	I_{cp}
0	116.4	21.90 KV	72.2 KW	11.4 A
48	109.6	13.75 KV	30.0 KW	6.9 A

From this example and the theoretical graphs it can be seen that the biggest impact of the voltage sag is on the average power of the system.

The energy stored in the capacitor network per cycle is given by Equation 2.

$$E_s = \frac{1}{2} C [V_c(T_r)^2 - V_o^2] \quad (2)$$

Equation 3 below gives the energy input from the power supply per cycle.

$$E_I = V_{av} I_{av} T_r \quad (3)$$

Where V_{av} and I_{av} are the average input voltage and current respectively and T_r is the repetition period.

The average of the input voltage given by Equation 1 is

$$V_{av} = I_{bb} (1 - K I_{av}) \quad (4)$$

and the average input current is (Ref 1:362).

$$I_{av} = f_r C [V_c(T_r) - V_o] \quad (5)$$

where f_r is the repetition frequency or $f_r = \frac{1}{T_r}$.

The efficiency of DC charging is given by the ratio of the energy stored in the network in one cycle to the input energy from the power supply during that cycle.

Dividing Equation 2 by Equation 5, substituting the expression of I_{av} given by Equation 5, and simplifying we get the following expression for the efficiency.

$$\eta_c = \frac{V_c (T_r) + V_o}{2 V_{av}} \quad (6)$$

Using equations 4 through 6 the efficiency for the ideal case of Table 1 is 98.6% and for the other case it is 88.1%. Therefore the efficiency is reduced, which is another undesirable effect of the voltage sag.

Figures 8 through 12 show the current and voltage waveforms for the same circuit parameters. These are plotted for sag constant equivalent to 0, 10, 15, 50, and 45 percent sagging respectively. The first cycle on each plot is for zero initial voltage and the second cycle is for an initial voltage $V_o = -0.1 V_c(T_r)$.

From the plots on the following pages we note that the shape of the charging current changes and the peak to average current increases for a larger sag on the input voltage. This increases the heat losses throughout the circuit. Note also that the capacitor will charge to a smaller voltage. It is important to recognize that T_r is different for each case and increases with increasing sag.

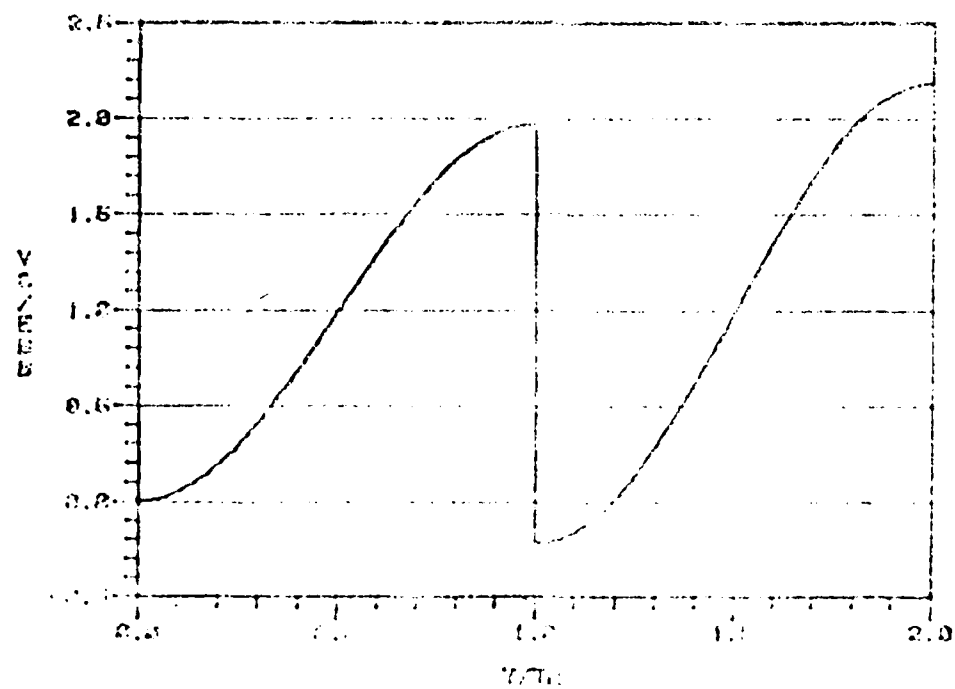
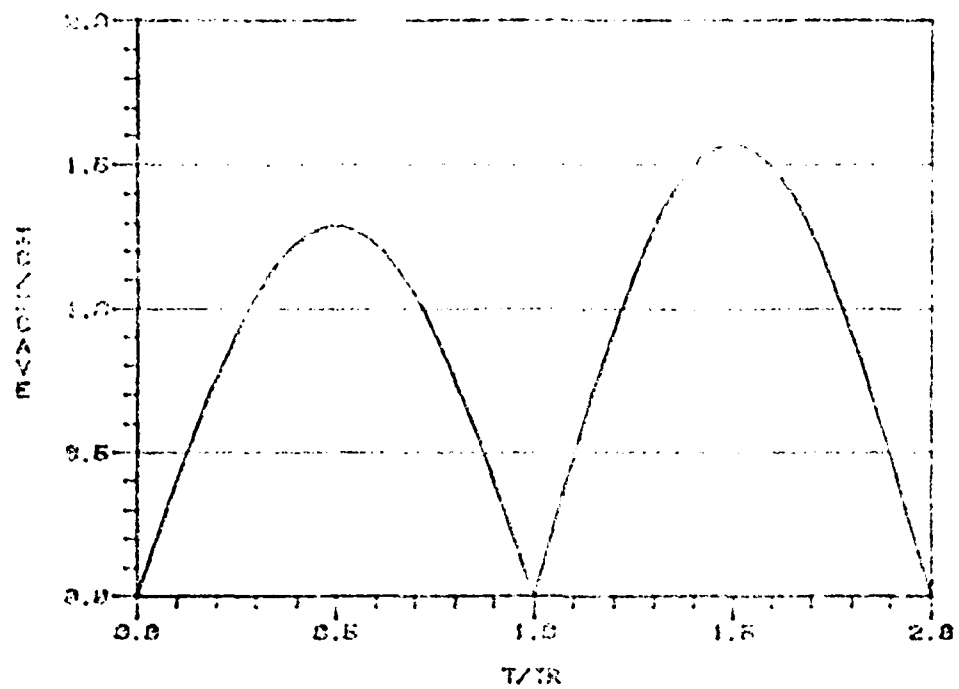


Figure 8 Theoretical Plots of the Charging Current and Capacitor Voltage for 5% Sag on Input Voltage

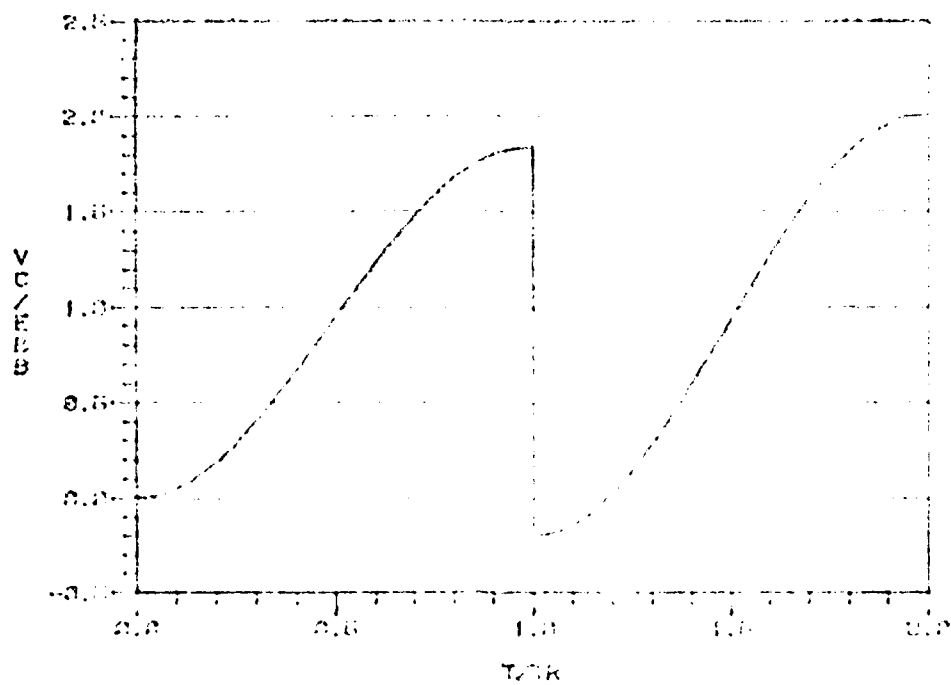
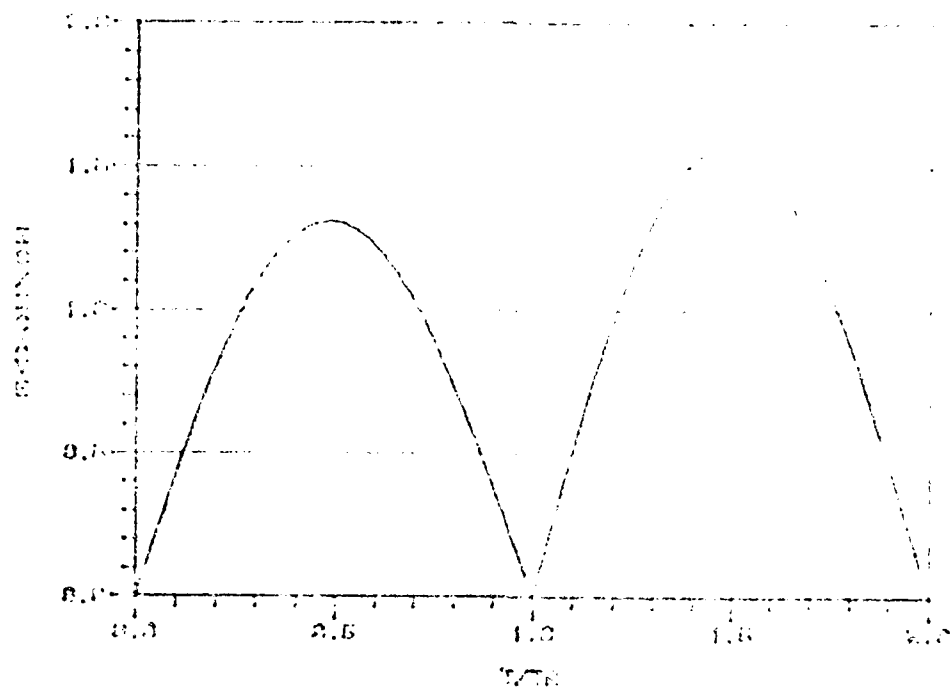


Figure 9 Theoretical Plots of the charging current and Capacitor Voltage for 10% Sag on Input Voltage

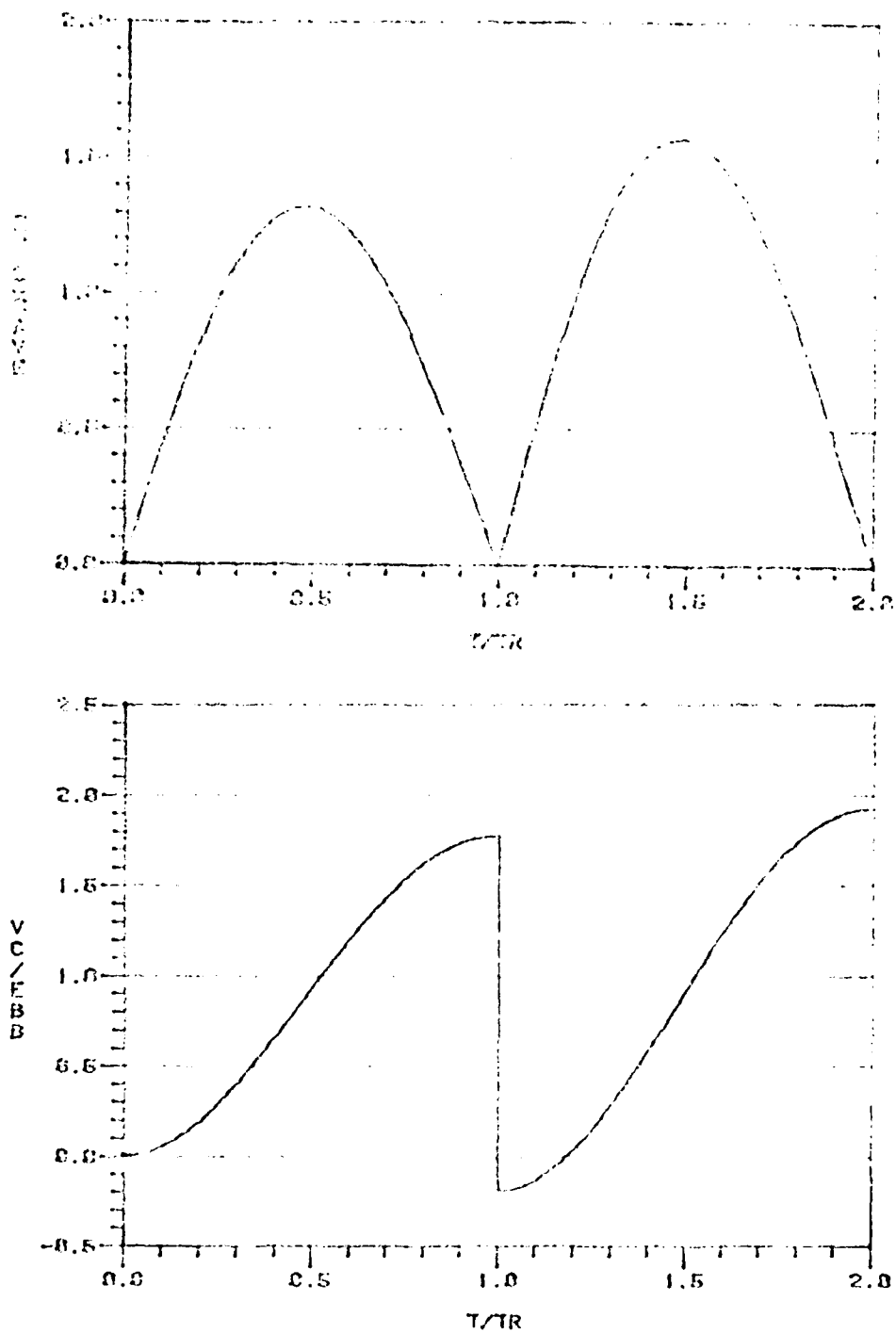


Figure 10 Theoretical Plots of the Charging Current and the Capacitor Voltage for 15% Sag on Input Voltage

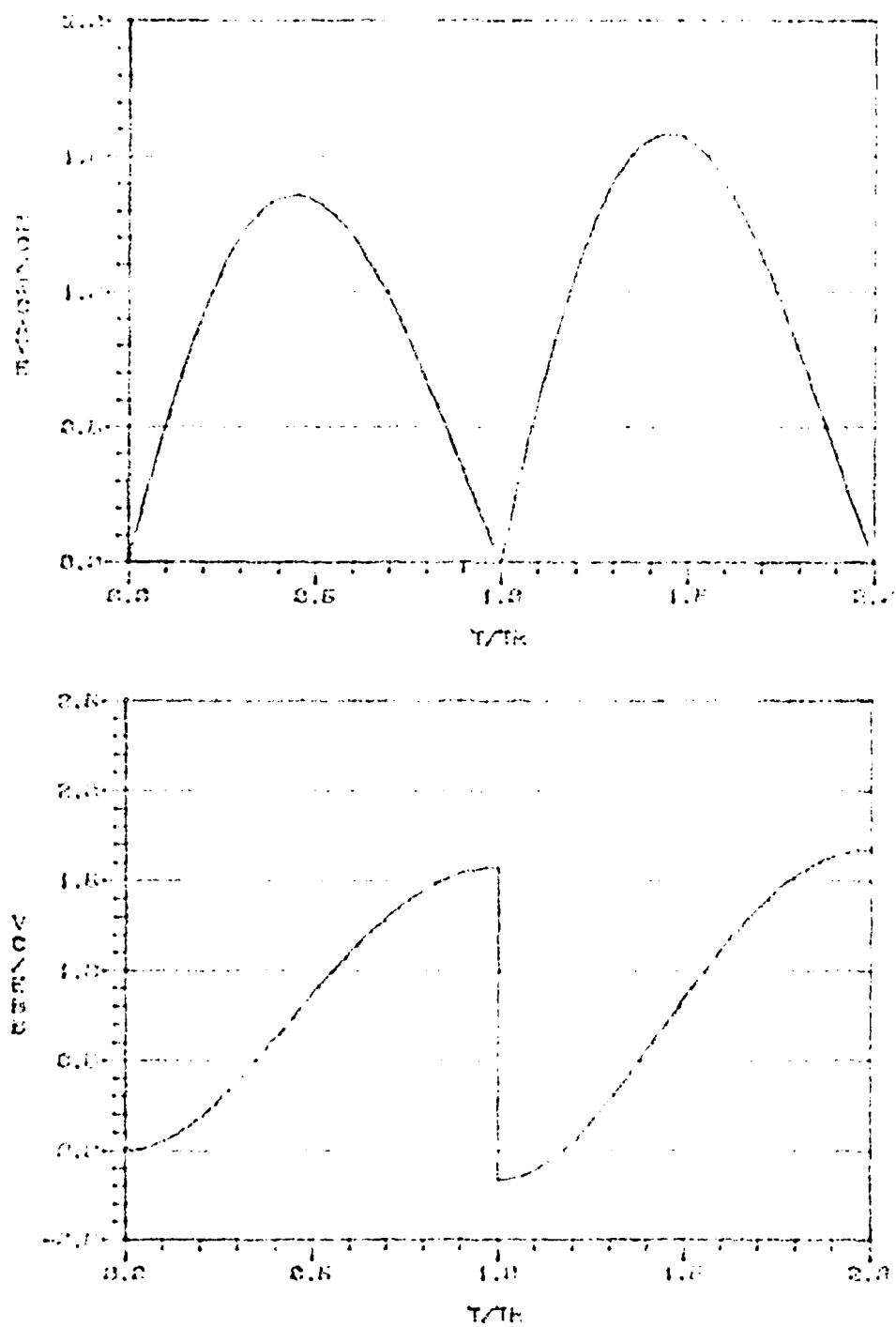


Figure 11 Theoretical Plots of the Charging Current and Capacitor Voltage for 50% Sag on Input Voltage

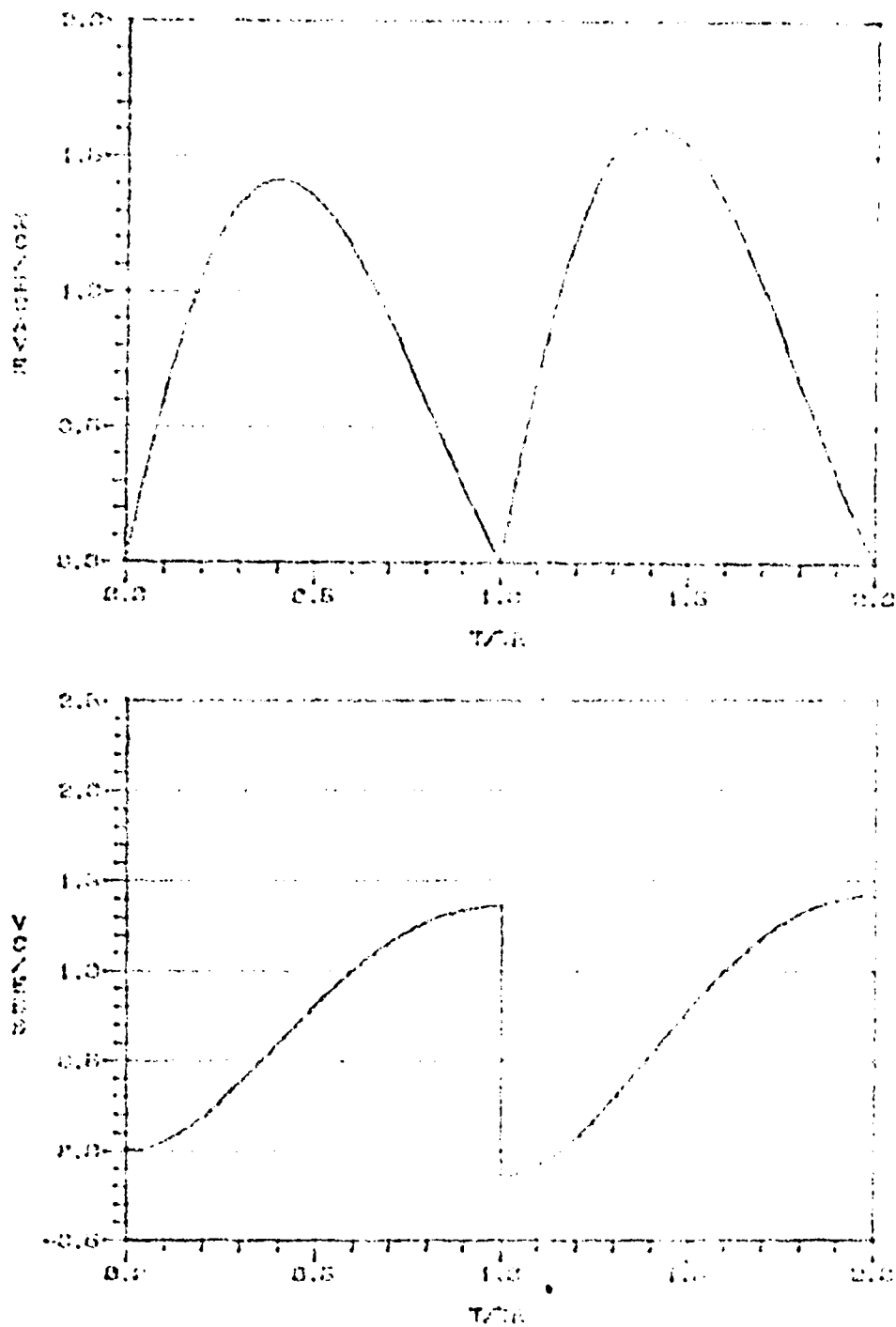


Figure 12 Theoretical Plots of the Charging Current and Capacitor Voltage for 45% Sag on Input Voltage

Experimental Equipment and Instrumentation

Figure 13 below is a block diagram of the experimental system.

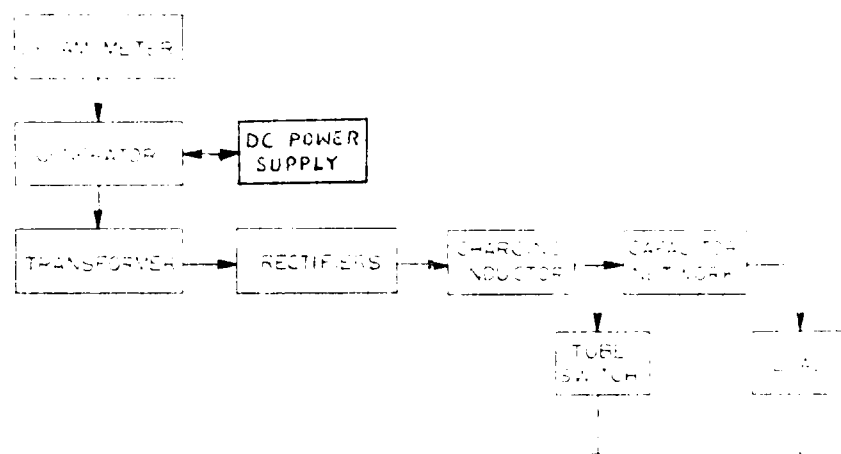


Figure 13 Block Diagram of DC Resonant Charging System

The prime mover was a 150 horsepower General Electric DC dynamometer. The generator was a DOD standard 15KW, 400HZ generator. A DC power supply was used for the generator exciter instead of a voltage regulator. The transformer had a voltage step-up ratio of 11:1. The liquid cooled full-wave bridge rectifier assembly had a nominal current capacity of 3 amperes per leg and a peak reverse voltage of 64kV. The charging inductor, capacitor network, tube switches, and the load were connected in the circuit shown in Figure 14.

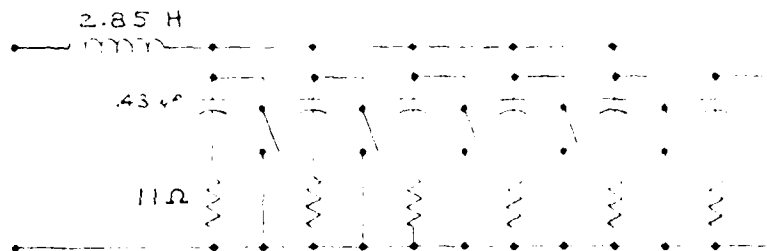


Figure 14 DC Resonant Circuit

Each of the six stages shown had a 0.43 μ f capacitor and an 11 ohm load resistor. The charging inductor was 2.85 Henrys. The tube switches were EG & G hydrogen thyratrons model HY-1A with a peak forward voltage of 20KV and a peak current of 0.5KA.

The schematic diagram of Figure 15 shows the test circuit with the test points marked a thru e.

The 0.0075 μ f capacitor was connected at the output of the full-wave bridge rectifier to protect the diodes from damage by a voltage spike.

Two high voltage contactors were used in the operation of the pulser. The line contactor K2 controlled the pulsing by opening or closing the DC bus into the pulser. The "dump"

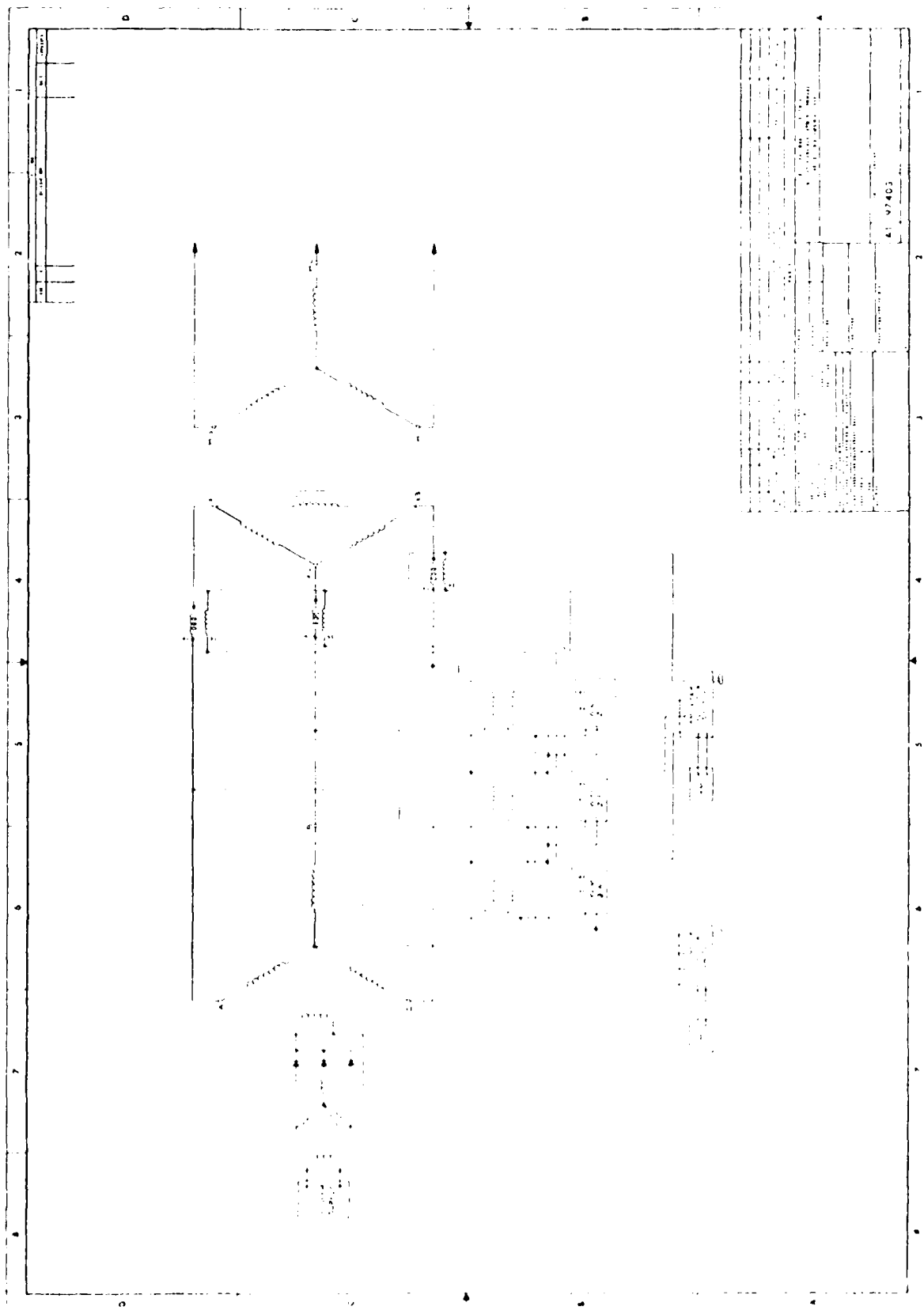


Figure 16 Schematic of Generator Instrumentation

contactor K4 closed after K2 opened so that any remaining voltage on the network was discharged thru a 7.5K resistor.

Note that a diode was connected between the charging inductor and the capacitor network. This is to prevent a current in the direction of the inductor when the pulser is discharged at a rate slower than resonance. Otherwise a high voltage spike is reflected back to the rectifiers and damage may occur.

The instrumentation diagram for the generator is shown in figure 16. This made it possible to read the average values of the phase voltage, current, and power delivered by the generator at all times.

Description of Pulser

A schematic diagram of the pulser built by LEAPCON is shown in figure 17.

A small inductance of approximately 20 μ h in series with the thyratrons was used to set the voltage in the capacitors to an initial negative value.

Metal oxide varistors (MOV) were used to suppress any high-voltage, high-frequency transients to vital components of the system.

The triggering circuit for the tubes consists of a function generator whose output is connected to the thyatron driver. The frequency of pulsing is set by the function generator. The output of the driver is connected through a matching transformer to a 140 Ω resistor and an MOV connected

in parallel. One output terminal of the transformer secondary is grounded to the chassis and from the other terminal a coaxial cable connects to a 300Ω resistor on the grid of each tube. This arrangement proved to be susceptible to noise and led to false triggering of the thyratrons.

The heater circuit for the hot-cathode thyratrons is composed of a transformer and filament choke as shown in the schematic.

A big current transformer was used to monitor the load current and a 0.1 Ω resistor on the low voltage return with an ammeter was provided for average charging current readings.

Both the load return and the chassis were brought together to one point and grounded to the building ground.

Modifications Made to the Pulser

Electro-magnetic coupling, or transients conducted thru the electrical connections, were causing the tubes to pre-fire when the line contactor k2 was closed. A high voltage, high frequency voltage spike was observed in the grid of the false-triggered tube.

To prevent this some signal lines were re-routed away from high voltage lines and duplicate grounds were connected to eliminate any possible ground loops. This reduced the problem but did not eliminate it. Finally six MOVs were connected, one to each tube from grid to cathode and the false triggering was eliminated.

This proved the importance of the physical layout of

the components and the proper routing and shielding of electrical signal lines in this type of system.

Operation of Pulser

With the generator running at rated speed and the line contactor K2 open, excitation was applied to bring the DC voltage to the desired level. Then the "pulse" command was given. The dump contactor K1 opened, the line contactor K2 closed, and the pulser operated. At the command "stop", K2 opened and then K1 closed to discharge the energy left in the network. Pulsing frequency was adjusted with the function generator.

General Approach

The pulser was operated to collect data in the form of readings and photographs of oscilloscope traces.

When a disagreement between theoretical expectation and measured performance was found, an investigation into the cause was made. In each case either hardware malfunctions were corrected or additions or corrections to the theory were made.

The first part of this report presents the theory of DC resonant charging. A discussion of the generator and its forms is followed by the analysis of the DC voltage surge. The equipment and instrumentation used to carry out the results of the tests are presented.

The second part of the report presents the theory of AC resonant charging. The experimental set up is described and observations of the operation of this system are discussed. No data was collected on the AC resonant system since problems with the triggering circuit were not solved in time for this report.

Results

Prime Power System

Generator

Figure 18 and 19 are photographs of the generator voltage and current, and the transformer secondary voltage and current (see Figure 15).

The ripple caused by the commutation of the current on the rectifiers is seen on all of these waveforms. One charging cycle has a duration of 9.4 msec compared to 2.5 msec for one generator cycle. So one charging cycle is almost four generator cycles. This can be clearly seen in Figure 18a where every four cycles the waveform of the current is repeated. These photographs correspond to 15kw output power from the generator.

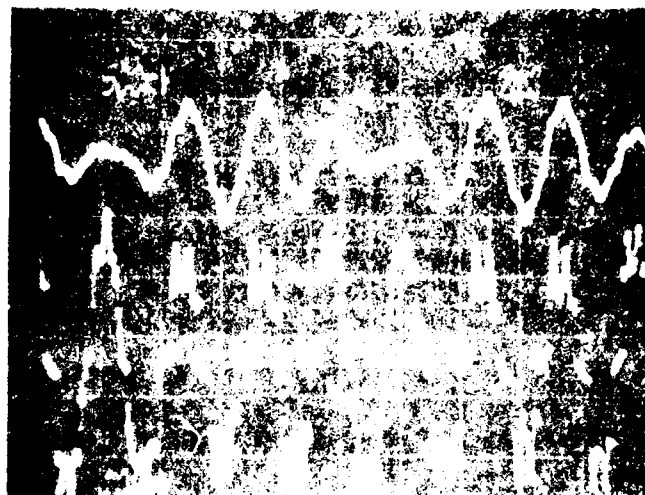
Vibration and Heating

The generator vibrated at the pulsing frequency. The torque pulsations were caused by the load current pulsing. Also because of the irregular generator voltage and current waveforms the generator heated faster since this caused increased losses on the windings.

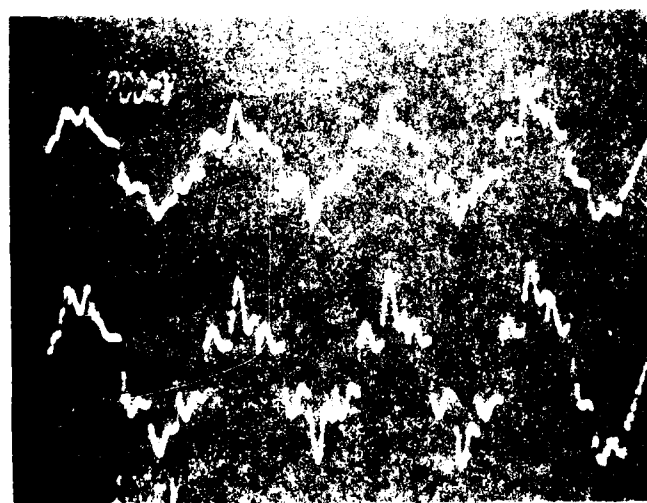
Voltage Regulator

Figure 20 shows scope traces of the input voltage (top trace) and the capacitor network voltage (bottom trace).

The oscillations on both voltages were caused by the voltage regulator. As seen on the picture the oscillations damp to a smaller magnitude but continue to about the

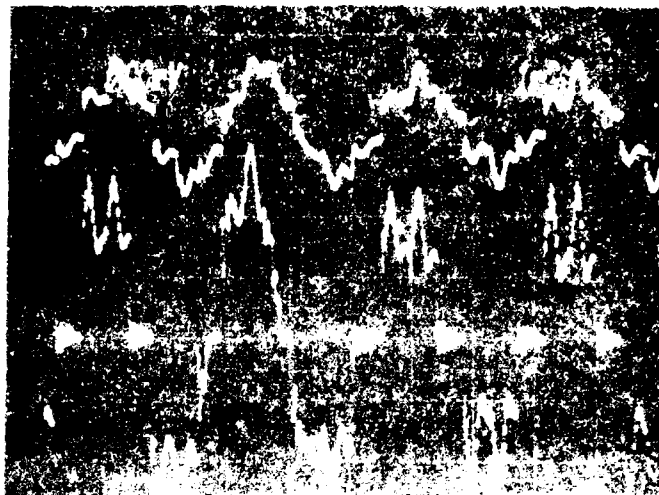


a) Gene 1
1'



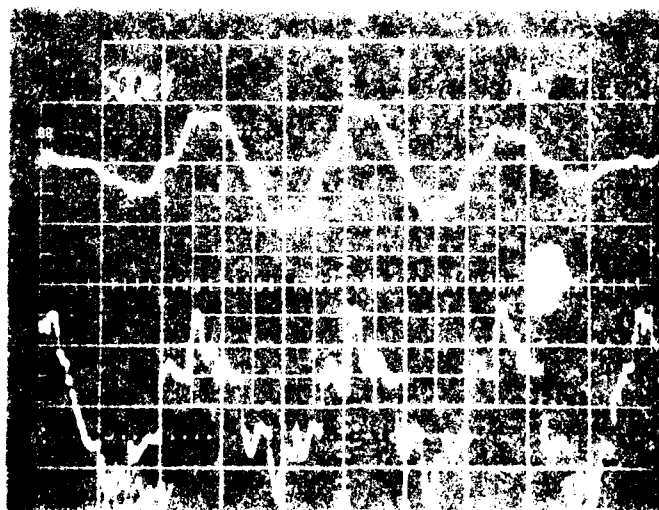
b) Gene 2
Seq 1

Gene 2
Seq 2 (div)



a) 1000
Sec

1000
ml



b) 1000
Sec

1000
ml

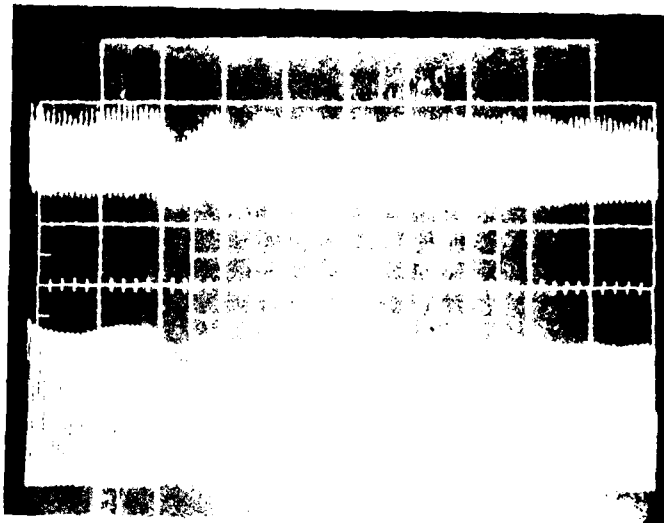


Figure 20 Scope Traces for the Pulser
(Test Points C and D respectively on Figure 15)

operation of the pulser. The reason for this malfunction was not investigated and a DC power supply was connected in place of the voltage regulator for the experiments.

Sag on Output Voltage

Figure 21 is a scope trace for the output voltage (top trace) and the inverted charging current (bottom trace). The output voltage sag follows the shape of the current very closely.

The frequency of the ripple on the output voltage is 2400Hz. Because of the big charging inductance the voltage will be equivalent to a DC voltage with a sinusoidal sag following the current waveshape. This criteria was used for the theoretical analysis.



Figure 21 (scope trace of $\frac{dV}{dt}$ on figure 17)

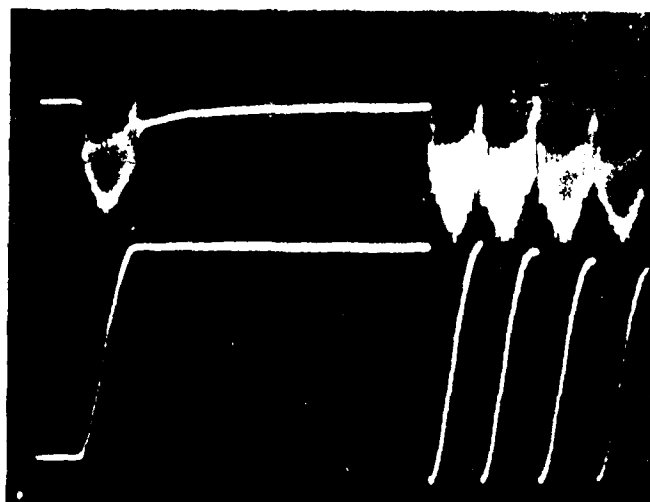


Figure 22 (scope trace of $\frac{dV}{dt}$)

the way to increase the output voltage is to increase the generator frequency. Figure 23 shows the capacitor network voltage and the input voltage to the pulser for three different frequencies.

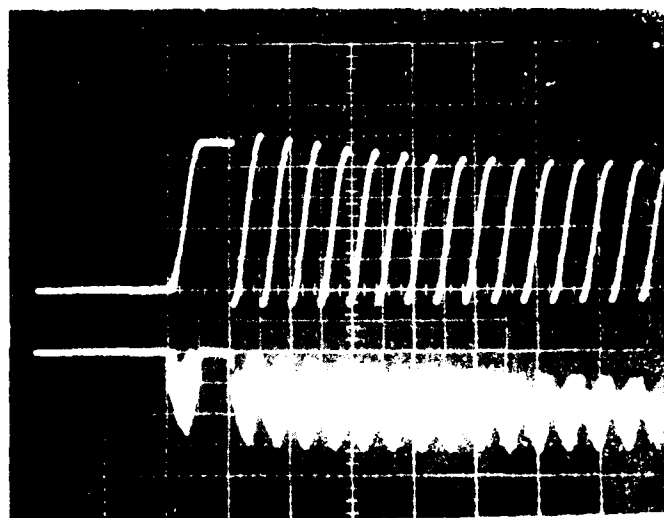
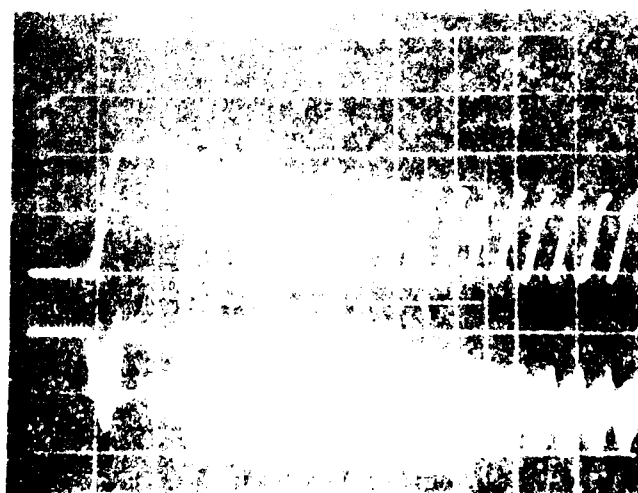
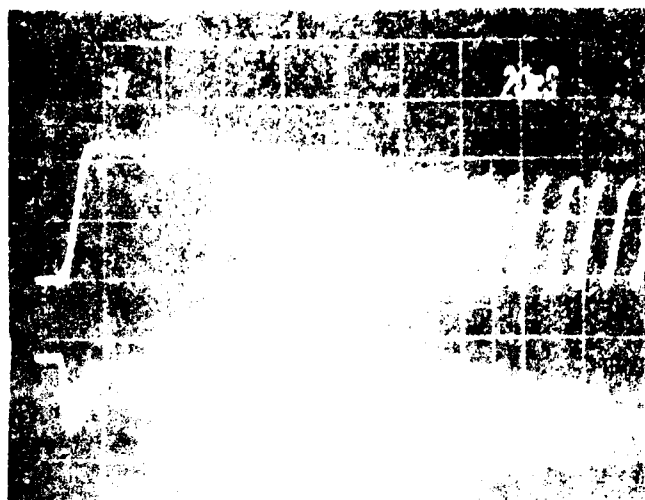


Figure 23. Scope Traces for a 100-ohm pulser at the Best Point of Load Compensation.

The change in generator frequency changes the input impedance. For the lower frequencies the input impedance is lower and the voltage drop across the network is lower. As the frequency is increased the network impedance increases and the voltage drop across the capacitor network increases. The voltage drop across the capacitor network is a function of the input voltage and the input impedance. The voltage drop across the capacitor network is a function of the input voltage and the input impedance.



few pulses and then both voltages remain at a constant peak level. This is because the generator has constant excitation and when the generator is loaded the average output voltage falls to a lower value. Another observation from the photographs is that the magnitude of the ripple on the bus voltage is smaller for 400 Hz than for the other two frequencies.

Pulser Performance

Before delivery to MERADCOM, where this investigation took place, the pulser was tested at ERADCOM to make sure it worked properly. The prime power for ERADCOM is a transformer rectified high voltage power line with a bank of capacitors to provide a stiff DC voltage.

Resonance frequency was measured at 117 Hz and the peak voltage in the capacitors was 17KV for a DC input voltage of 8KV. This can be taken as the control test since the input was for all matters an infinite DC bus.

Network Voltage and Charging Current

Figure 25 shows the DC bus voltage, or input voltage, and the charging current for 29KW generator output power. By visual inspection of the scope traces of Figure 25 the following values were obtained for this case:

$$E_{bb} = 11.5KV$$

$$K_{\alpha} = 0.50$$

$$I_{cp} = 6.6A$$

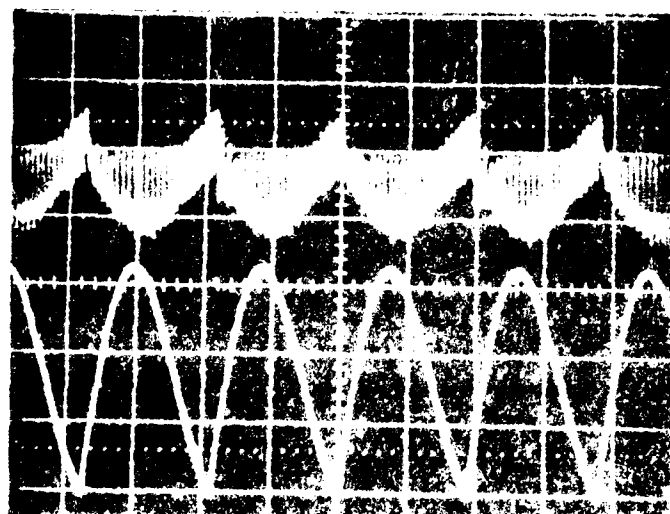


Figure 1. $\text{V}_{\text{m}}^{\text{max}}$ and $\text{V}_{\text{m}}^{\text{min}}$ vs. $\text{V}_{\text{m}}^{\text{avg}}$

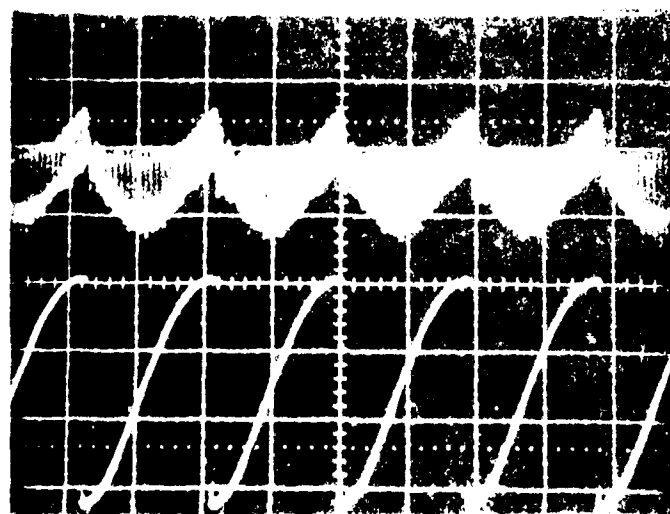


Figure 2. $\text{V}_{\text{m}}^{\text{max}}$ and $\text{V}_{\text{m}}^{\text{min}}$ vs. $\text{V}_{\text{m}}^{\text{avg}}$

The resonance frequency was 106.6Hz and $P = 0.055$ for this system. The computer calculated value of $V_c(I_P)$ was 14.8KV. Figure 26 shows the DC bus voltage and capacitor voltage for this case. The actual value of the capacitor voltage was 15.0KV which is very close to the calculated value the theoretical peak charging current was 7.2 AMP and the average power was 35.0KW.

Resonance Frequency

The resonance frequency did not change with power level. A universal bridge was used to measure each of the six capacitors and the total capacitance was 2.58 μ F. The inductance was measured by applying a high voltage at 400 Hz and measuring voltage and current to obtain impedance. The inductance obtained by this method was 2.85 henrys and the resistance of the inductor was 6.5 ohms. These values for the circuit components yield a resonance frequency of 117.1 Hz for no sag. This is very close to 117 Hz measured at ERADCOM.

Table 2 below summarizes the actual and calculated values for two cases, third case is for no sag of the input voltage and is included for contrast.

Theoretical values were obtained with the first computer program. Another case is presented in Appendix C.

TABLE 2 Comparisons of Actual Values vs. Calculated Values

E _{bb}	Calculated				Measured			
	V _c (T _r)	P _{av}	I _{cp}	T _r	V _c (T _r)	P _{av}	I _{cp}	T _r
8KV	10.5KV	17KW	5.9A	108.3	9.6KV	15kW	4.0	106.6
11.5KV	11.8KV	35kW	7.2A	108.3	15.0KV	29kW	6.6	110.6
11.5KV	24KV	89KW	12A	117.4	-	-	-	-

III. AC Resonant Charging

Theory

Introduction

AC resonant charging systems are less commonly used than DC resonant charging systems. There are many reasons for this, the concept of AC resonant charging is considerably more complicated and poses strict timing and control requirements. A major advantage of this alternative method is that it does not introduce torque pulsations on the generator at the pulse repetition rate. As the excitation voltage and current waveforms are sinusoidal the pulsed power output can be controlled by varying the generator field current (Ref. 1:392).

As more studies are completed on AC resonant charging, the more attractive this alternative method becomes for pulsed power supplies (Ref. 2).

Analysis

An AC charging circuit can be represented as in Figure 26.

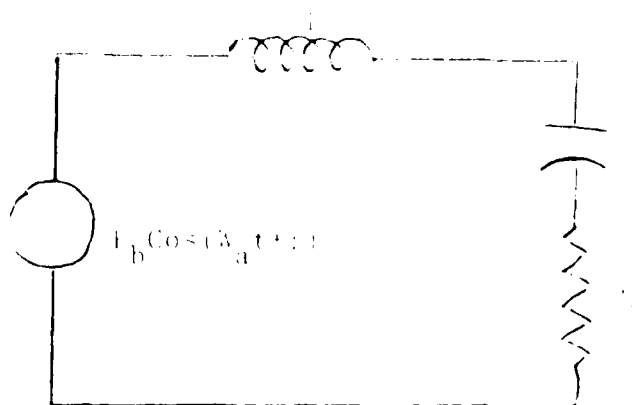


Figure 26. AC Charging Circuit

The equations for AC resonant charging are found in reference 1 chapter 9.4.5. These equations are not presented here since they would not contribute to the scope of this discussion.

Half cycle AC resonant charging was used in the tests. The circuit resonance frequency has to be equal to the alternator frequency, or

$$\omega = \omega_a$$

The condition for resonance is (Ref 1:385)

$$1 - L\omega^2 = 0 \quad (8)$$

The voltage stepup ratio at the time of discharge is for half cycle charging (Ref 1:388)

$$\frac{V_c(\pi)}{E_b} = \frac{\pi}{2} \left(1 - \frac{\pi}{4Q}\right) \sin \phi + \frac{V_o}{E_b} \left(1 - \frac{\pi}{2Q}\right) \quad (9)$$

Where E_b is the peak AC input voltage, ϕ is the phase of the input voltage, V_o is the initial capacitor voltage, and

$$Q = \frac{L\omega_a}{R} = \frac{1}{RC\omega_a} \quad (10)$$

Equation (9) is true for $\pi/2Q \ll 1$. For negligible losses

Equation (9) becomes

$$\frac{V_c(\pi)}{E_b} = \frac{\pi}{2} \sin \phi + \frac{V_o}{E_b} \quad (11)$$

Equation (11) and other solutions in reference 1 indicate that for maximum efficiency ϕ has to be close to $\pi/2$. All this means is that charging should start at or near the beginning of a half cycle of the input voltage.

The difference between the resonance frequency of the individual circuits and the alternator frequency can be up to 10% without significant effect on the pulser operation (Ref 5). This is a great advantage given that a high power AC resonant system requires many resonant circuits that need to be tuned at the alternator frequency.

Experimental Equipment and Instrumentation

Figure 27 is a block diagram of the experimental system.

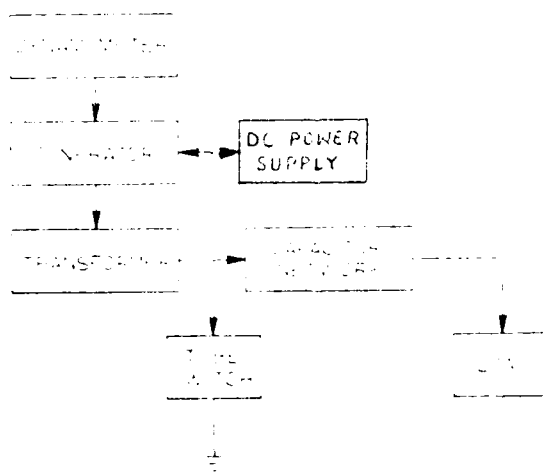


Figure 27 Block Diagram of AC Resonant Charging System

The dynamometer, generator, and DC power supply were the same used for DC resonant charging. Three transformers with a voltage step-up ratio of 18.5:1 were connected in Y-Y configuration. These three high leakage transformers provided the total charging inductance. The AC resonant charging circuit is shown in Figure 28.

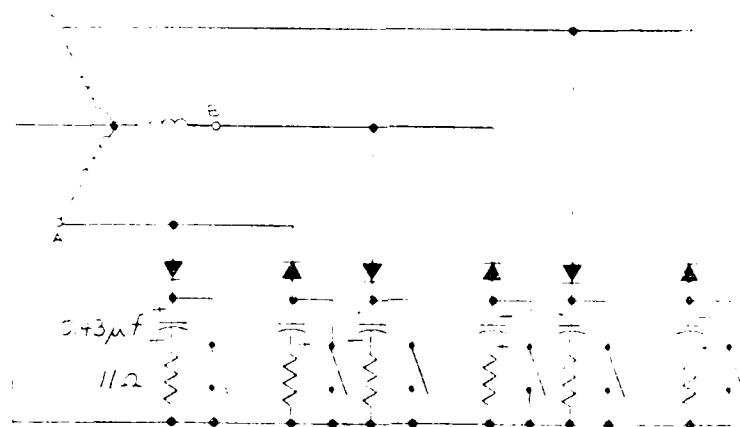


Figure 28 AC Resonant Circuit

This circuit has two 0.43 μ f. capacitors per stage, one for each half cycle of the phase voltage. The diodes were stacks with a total PRV of 50KV and a nominal current of 20 AMPS. The load for each of the six stages was an 11 ohm resistor. The tube switches were EG&G hydrogen thyratrons model HY-1A with a peak forward voltage of 20KV and a peak current of 0.5KA.

The diodes were connected so that the capacitor charged with the positive half cycle of the plate voltage and the other capacitor charged with the negative half cycle. In this way the alternator was continually discharging and recharging at the repetition rate. Each capacitor is discharged during the next half cycle after recharging.

High voltage scope probes were used to monitor input voltage and capacitor voltage.

Description of Pulse

The generator has an internal discharge circuit which is controlled by a switch. The switch is controlled by a pulse from the input of the oscilloscope. The pulse is applied to the input of the oscilloscope and the output of the oscilloscope is connected to the input of the generator.

The generator has an internal discharge circuit which is controlled by a switch. The switch is controlled by a pulse from the input of the oscilloscope. The pulse is applied to the input of the oscilloscope and the output of the oscilloscope is connected to the input of the generator. The generator has an internal discharge circuit which is controlled by a switch. The switch is controlled by a pulse from the input of the oscilloscope. The pulse is applied to the input of the oscilloscope and the output of the oscilloscope is connected to the input of the generator. The generator has an internal discharge circuit which is controlled by a switch. The switch is controlled by a pulse from the input of the oscilloscope. The pulse is applied to the input of the oscilloscope and the output of the oscilloscope is connected to the input of the generator.

Operation of Pulser

Excitation was applied with the alternator at rated speed. When the plate voltage was at its maximum



Figure 25. Schematic diagram of W. Fulser

level for the sensing circuit, the logic box started triggering the thyratrons at the proper time. The output power of the pulser was regulated by controlling the exciter current.

Results

Resonance Frequency

The resonance frequency of one of the circuits is calculated next.

From Appendix D the leakage reactance of one transformer was 64.44 percent, or

$$Z_L = \frac{64.44}{100} \cdot \frac{4440 \text{ v}}{4.5 \text{ a}} = 636 \text{ ohms}$$

The leakage inductance for 400 HZ was therefore

$$L_t = \frac{636 \text{ } \Omega}{2\pi(400) \text{ r/s}} = 0.253 \text{ HENRYS}$$

Also from Appendix D the alternator leakage reactance was 0.059 per unit, or

$$Z_{La} = 0.059 \cdot \frac{240 \text{ v}}{26 \text{ a}} = 0.545 \text{ ohms.}$$

The transformer voltage ratio was 18.5 so at the secondary the alternator leakage inductance was

$$L_a = (18.5)^2 \cdot \frac{0.545 \text{ } \Omega}{2\pi(400) \text{ r/s}} = 0.074 \text{ HENRYS}$$

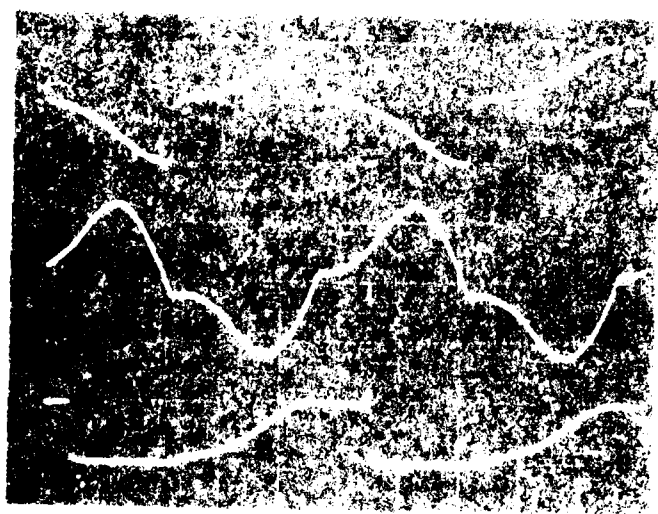
The total charging inductance was then

$$L_c = L_t + L_a = 0.327 \text{ HENRYS}$$

and the resonance frequency with $C = 0.45 \text{ } \mu\text{F}$

$$f = \frac{1}{2\pi \sqrt{(0.45 \times 10^{-6}) (0.327)}} = 4.1 \text{ HZ}$$

which is very close to 400 HZ.



before entering the logic triggering box. Inside the logic box a zero crossing detector circuit and a timing circuit for each phase generated the triggering signals. The delay of the trigger pulse was set by adjusting the timers.

When the magnitude of the input voltage went above that shown in Figure 50 the triggering circuit generated multiple trigger signals per half cycle discharging the capacitors before they reached maximum voltage. This was a malfunction caused by the electronic logic circuit, this problem was not solved in time for this study.

Since the logic box worked only for very low voltage, and therefore low power, no data was collected on the system performance. General observations of this system are presented in the next chapter.

IV Conclusions and Recommendations

DC resonant charging is better known by people in the field of pulse power and is used more commonly than AC resonant charging. The problems presented by DC resonant charging on this study were vibration of the generator at the pulse repetition rate, irregular voltage and current waveforms in the generator, and lower performance of the DC resonant circuit due to input voltage sag. On the other hand, a DC resonant charging system is rather simple to construct and simple to trigger and control.

An AC resonant charging system has more hardware than an equivalent power DC resonant system and pulsing frequency is limited by the generator frequency. Also controls and triggering are far more complicated.

AC resonant charging does not cause a negative impact on the generator and this makes it very attractive.

Because of the high voltages and physical proximity of the components electromagnetic phenomena will cause problems for the signal lines. Proper shielding and routing of these lines together with transient suppressors (like MOV's, filters) have to be used.

The generator voltage control for DC resonant charging was a problem on the experiments and the alternative of feedforward voltage control should be considered. The sag of the DC bus voltage needs to be minimized for high performance and efficiency on a DC resonant charging system of this kind.

If this is done, DC resonant charging will be a satisfactory method for this kind of power supplies, except possibly for airborne power units.

More research on AC resonant charging is needed, especially on triggering schemes. AC resonant charging is without doubt a better interfacing method from the prime power system point of view.

Recommended Additional Work

DC Resonant Charging

Investigate the cause of instability of the voltage regulator and consider the approach of feedforward voltage control.

Define what system parameters, and how they do, determine the magnitude of the DC voltage sag. Suggest changes in the system to minimize this sag.

Install MILADCOM controls and operate the system, make necessary changes to improve the system.

AC Resonant Charging

Correct triggering circuit malfunction. Study the effect of AC resonant charging on the generator. Study pulser performance and compare to theory.

Bibliography

1. Pulse Generators, G. N. Glasoe and J. V. Lebacqz;
Radiation Laboratory Series First Edition, McGraw-
Hill Book Company 1948 (TK7803.M3).
2. "A System Approach to Lightweight Modulator Design for
Airborne Applications", Major F. S. Zimmerman, et al.
3. O'Loughlin, J.P., Electrical Engineer, Personal Interview,
Air Force Weapons Laboratory, Kirtland Air Force Base,
New Mexico, December 4, 1980.

APPENDIX A

Mathematical Analysis of DC Resonant Charging

The differential equation for the circuit of Figure 1 is

$$L \frac{d^2 q}{dt^2} + R \frac{dq}{dt} + \frac{q}{C} = V(t) \quad (A-1)$$

where q is the instantaneous charge on the network.

The input voltage to the network $V(t)$ was represented as in Equation (1) repeated here for convenience.

$$V(t) = E_{bb} (1 - K i_c(t)) \quad (1)$$

where $i_c(t)$ is the charging current as a function of time, K is a constant and E_{bb} is the peak input voltage.

Figure A-1 shows the plot of Equation (1) for two charging cycles.

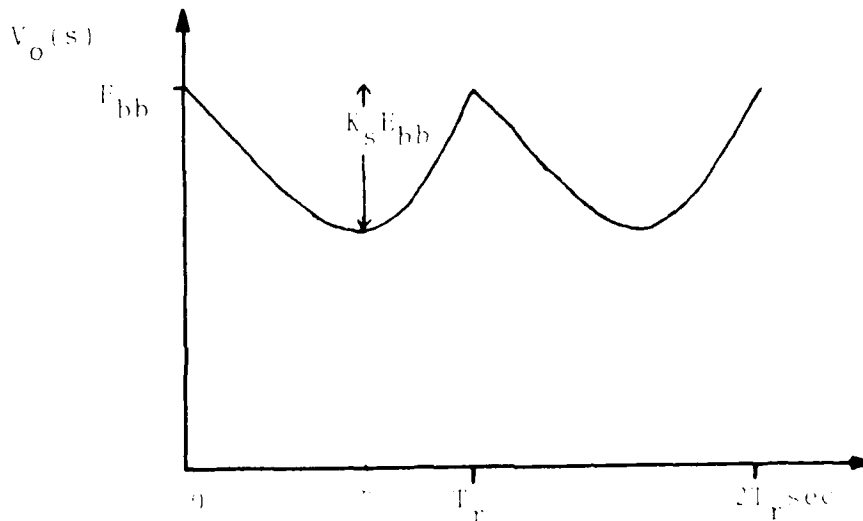


Figure A-1 Plot of Eq(1) for Two Charging Cycles

The constant K is defined by Equation (A-2) below.

$$K = \frac{K_s}{I_{cp}} \quad (A-2)$$

where I_{cp} is the peak value of the charging current. At time $t = 0$, $i_c(t) = I_{cp}$ and equation (1) is then

$$V(t) = E_{bb} (1 - K_s)$$

therefore K_s is the sagging constant and has values from zero to one. For example, if $K_s = 0.1$ the input voltage $V(t)$ has a sagging of 10%, if $K_s = 0.5$ the sagging is 50% and so on.

Substituting $\frac{dq}{dt}$ for $i_c(t)$ and combining Equations (A-1) and (1) we obtain, after rearranging terms,

$$L \frac{d^2q}{dt^2} + (R + \frac{K_s}{I_{cp}} E_{bb}) \frac{dq}{dt} + \frac{q}{C} = E_{bb} \quad (A-3)$$

now let

$$K = \frac{K_s}{I_{cp}} ; b = \frac{R + K E_{bb}}{2L} \quad \text{and} \quad \omega_o^2 = \frac{1}{LC}$$

then Equation (A-3) becomes

$$\frac{d^2q}{dt^2} + 2b \frac{dq}{dt} + \omega_o^2 q = \frac{1}{L} E_{bb} \quad (A-4)$$

Equation (A-4) is similar to that obtained by Gilmore and Lebacqz (Ref. 1:356-360) the only difference is in the definition of the constant b . The solutions for Equation (A-4) are

$$i_c(t) = \frac{E_{bb} - V_o}{\omega L} e^{-bt} \sin \omega t + I_o e^{-bt} \left(\cos \omega t - \frac{b}{\omega} \sin \omega t \right) \quad (A-5)$$

and

$$V_c(t) = E_{bb} - (E_{bb} - V_o) e^{-bt} \left(\cos \omega t + \frac{b}{\omega} \sin \omega t \right) + \frac{I_o}{\omega C} e^{-bt} \sin \omega t \quad (A-6)$$

where

V_o - Initial capacitor voltage

I_o - Initial inductor current

$\omega = \omega_o^2 - b^2$ - resonance frequency

Equations (A-5) and (A-6) are the expressions for the charging current and capacitor voltage respectively.

Evaluating Equation A-6 at $t = T_r = \frac{\pi}{\omega}$ we find the expression for the voltage in the capacitor at the time of discharge.

$$V_c(T_r) = E_{bb} + [E_{bb} - V_o] e^{-b \frac{\pi}{\omega}} \quad (A-7)$$

The maximum value of Equation (A-5) is found by differentiating the expressions and setting it equal to zero. The initial current I_o is assumed equal to zero. This is correct because at resonance I_o is zero and near resonance I_o is a very small number. The time t at which Equation (A-5) has a maximum value is

$$\phi = \text{ARCTAN} \left(\frac{W}{R} \right) \quad (\text{A-6})$$

then

$$I_{cp} = \frac{I_{bb} V_o}{W R} e^{-bt} \sin \omega t \quad (\text{A-7})$$

In order to evaluate the constant b we need I_{cp} , but I_{cp} is a function of b . The way to solve this is to assume a value of $k = K_S / I_{cp}$ and evaluate b , then use that value of b with Equation (A-6) and (A-7) to find I_{cp} .

Multiplying the assumed value of k by the computed I_{cp} will give the value of the scaling constant K_S for which this calculation was made.

A small inductance was connected in series with the thyatron tubes to provide an initial negative voltage V_o . This initial voltage was proportional to the voltage in the capacitor at the discharge time. This factor was called p and was used for calculations in the two computer programs. Substituting $V_o = p V_c(T_P)$ in Equation (A-7) and solving for $V_c(T_P)$ we obtain,

$$V_c(T_P) = I_{bb} \frac{1 + \text{EXP}(-bT_P)}{1 - p \text{EXP}(-bT_P)} \quad (\text{A-10})$$

or solving for V_o ,

$$V_o = -I_{bb} \frac{1 + \text{EXP}(-bT_P)}{p \text{EXP}(-bT_P)} \quad (\text{A-11})$$

Equations (A-10) and (A-11) were used in the computer programs.

APPENDIX B

Computer Programs

Figure B-1 shows the first of the two computer programs developed to obtain theoretical solutions. This program calculated the resonance frequency, peak capacitor voltage, peak charging current, average current, average voltage, and average power for increasing values of input voltage sag.

The program required as input the value of the circuit components, the peak input voltage E_{bb} , and $p(=-V_o/V_p(T_r))$.

The output was the data displayed in Figure 1 through 7 in Chapter II.

Figure B-2 shows the second fortran program. This program calculated the ratio of charging current to average charging current and capacitor voltage to peak input voltage versus time.

The program required as input the value of the circuit components, peak input voltage, $P(=-V_o/V_c(T_r))$, constant $K(=K_s/I_{cp})$, and repetition frequency.

The constant K was found by running the other program first to obtain the set of plots for varying sag constant K_s . The value of peak current for the sag constant of interest was read from the proper curve and K was calculated. If the line where V_o is defined for the second time in the program (see arrow) is changed to $V_o = -PE_{bb} V_{cs}$ the program can be run for repetition frequencies higher than resonance.

This program runs for more than one cycle by storing the final value of the current as the initial value for the next cycle and resetting the voltage in the capacitor to a negative value proportional to the voltage at the time of discharge.

The output of this program was the data displayed in Figure 8 through 12 in Chapter II.

APPENDIX C

Additional Case

Figure (C-1) shows the DC bus voltage and the charging current for 15KW output power of the generator.

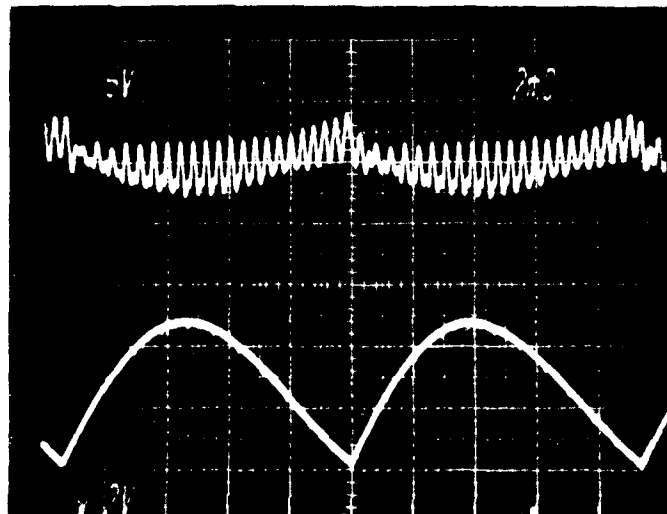


Figure C-1 Scope Trace of DC Bus Voltage (10P) and Charging Current (5KV/div, 2A/div)

From visual inspection of Figure C-1 the following values are obtained:

$$V_{bb} \approx 8KV$$

$$K_s \approx 0.50$$

$$I_{cp} \approx 1.6 AMP$$

the resonance frequency was 106.6Hz and $Q = 0.955$. The computer calculated value of $V_c(I_p)$ was 10.5 KV. Figure (C-2) shows the DC bus voltage and the capacitor voltage for this case. The actual value of the peak capacitor voltage was 9.6KV.

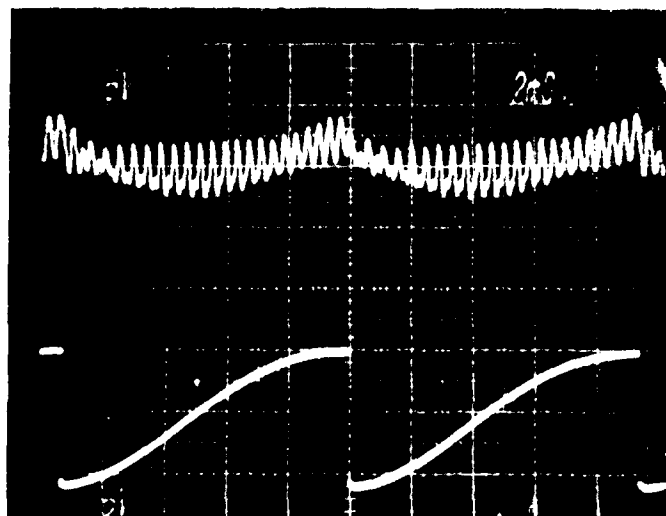


Figure C-2 Scope Trace of DC Bus Voltage (TOP) and Capacitor Voltage (5KV/div)

The theoretical peak charging current was 5.0 A/P, the average power 17kW, and the resonance frequency 108.5Hz.

APPENDIX D
Major Parts List

General

DYNAMO - GE 150 HP dynamometer

GENERATOR - 15 KW DOD Standard

400 HZ, 210 V 26A, 2000 RPM

THYRATrons - JAN 8613, 5MB Peak Power,

20KV Peak ANODE Voltage, 0.5KA

Peak Forward Current

DC Resonant

Transformer - 50KV, 400 HZ, 4467020W

Rectifiers - Liquid cooled Westinghouse

Rectifier assembly, 62 KV, PRA, 50 AMP nominal current

AC Resonant

Transformers - Three 400 HZ Transformers, 240:440V, 4.5 AMPS secondary nominal current, 64.44 62.82 64.23 pu leakage reactance and 4.25 4.20 4.17 pu resistance respectively.

Charging Diodes - rectifier stack with 50KV PRA, 50A nominal current.

Vita

Jaime Roberto Silva was born on 11 October 1956 in San Juan, Puerto Rico. He graduated from high school in Rio Piedras, Puerto Rico in 1974 and attended the University of Puerto Rico Mayaguez campus from which he received the degree of Bachelor of Science in Electrical Engineering in June 1979. Upon graduation he received a commission in the United States Air Force through the ROTC program and entered the School of Engineering, Air Force Institute of Technology in June 1979.

Permanent Address: 327 Barnard Street

Rio Piedras, Puerto Rico 00926

SECURITY CLASSIFICATION OF THIS PAGE (When Data Entered)

REPORT DOCUMENTATION PAGE		READ INSTRUCTIONS BEFORE COMPLETING FORM
1. REPORT NUMBER	2. GOVT ACCESSION NO.	3. REPORTING DATA NUMBER
DL A166 827		
4. TITLE (and Subtitle)	5. AUTHOR	
6. PERFORMING ORGANIZATION NAME	7. PERFORMING ORGANIZATION NUMBER	
8. PERFORMING ORGANIZATION ADDRESS	9. PERFORMING ORGANIZATION CITY	
10. PERFORMING ORGANIZATION STATE	11. PERFORMING ORGANIZATION COUNTRY	
12. DISTRIBUTION STATEMENT (of this Report)	13. DISTRIBUTION STATEMENT (of the abstract entered in item 4 of this Report)	
14. SUPPLEMENTARY NOTES		
11 DEC 1980		
15. KEY WORDS (Continue on reverse side if necessary and identify by block number)		
16. ABSTRACT (Continue on reverse side if necessary and identify by block number)		

16 JUN 1981

Medric C. Lynch

SECURITY CLASSIFICATION OF THIS PAGE (When Data Entered)

1. This document is classified "Secret" because it contains information that is so classified and its disclosure could result in the identification of sources, methods, or equipment of the intelligence community.

DATE
ILMED
-18-